Draft version June 2, 2026
Typeset using LaTeX **twocolumn** style in AASTeX7.0.1

Mass and Spin Growth of Very Massive Stars in Star Clusters Potentially Associated with Little Red Dots

Ataru Tanikawa [1], Masaru Shibata [2,3] and Kunihito Ioka [3]

[1] *Center for Information Science, Fukui Prefectural University, 4-1-1 Matsuoka Kenjojima, Eiheiji-cho, Fukui 910-1195, Japan*
[2] *Max-Planck-Institut für Gravitationsphysik (Albert-Einstein-Institut), Am Mühlenberg 1, D-14476 Potsdam-Golm, Germany*
[3] *Center for Gravitational Physics and Quantum Information, Yukawa Institute for Theoretical Physics, Kyoto University, Kyoto, 606-8502, Japan*

ABSTRACT

Using gravitational N-body simulations, we investigate the evolution of mass and spin for very massive stars (VMSs) in dense star clusters, which may be potentially associated with Little Red Dots (LRDs). Our results show that VMS masses can reach 10^3–$10^4\,M_\odot$, depending on the initial conditions of the host clusters. Notably, the VMS mass increases by up to a factor of three when accounting for the bloated state at the Hayashi track induced by stellar collisions, provided that this state is maintained at accretion rates exceeding $3\times10^{-2}\,M_\odot\,\mathrm{yr}^{-1}$. In all cases, the spin of the VMS, when normalized to the dimensionless black hole (BH) spin parameter, exceeds 10. While our model may overestimate VMS masses and spins due to the omission of post-main-sequence evolution and the loss of mass and angular momentum during collisions, we nonetheless demonstrate that VMSs formed in dense star clusters can be highly spinning. Such a rapidly spinning VMS is expected to collapse into an intermediate-mass BH surrounded by a massive accretion disk. This BH-disk system could trigger powerful explosions and emit burst gravitational waves, similar to those observed in GW190521 and GW231123, for which the remnant BH masses are estimated to be $\gtrsim 100\,M_\odot$.

Keywords: Star clusters (1567) – N-body simulations (1083) – Massive stars (732) – Gravitational wave sources (677)

1. INTRODUCTION

Very massive stars (VMSs) with initial masses of $\sim 10^2$–$10^4\,M_\odot$ are predicted to collapse into black holes (BHs) triggered by electron-positron pair-instability (Y. B. Zeldovich & I. D. Novikov 1971; C. L. Fryer et al. 2001; A. Heger & S. E. Woosley 2002). One of the primary formation channels for VMSs is runaway stellar collisions within dense star clusters (R. H. Sanders 1970; M. C. Begelman & M. J. Rees 1978; G. D. Quinlan & S. L. Shapiro 1990; S. F. Portegies Zwart et al. 2004; M. Giersz et al. 2015; F. P. Rizzuto et al. 2021; U. N. Di Carlo et al. 2021; L. Wang et al. 2022; E. González Prieto et al. 2022; M. S. Fujii et al. 2024; M. C. Vergara et al. 2025). In this scenario, multiple stars undergo successive collisions to form a single VMS before reaching the end of their stellar evolution. If such a VMS collapses into a BH of comparable mass, the resulting object would be classified as an intermediate-mass BH (IMBH). These IMBHs are potential candidates for ultra-luminous and hyper-luminous X-ray sources (e.g., H. Matsumoto et al. 2001; S. A. Farrell et al. 2009), and may explain the nature of the massive dark object recently identified at the center of ω Centauri (M. Häberle et al. 2024).

Recently, the *James Webb Space Telescope* (JWST) has identified a novel population of red, massive, compact objects known as "Little Red Dots" (LRDs; D. D. Kocevski et al. 2023; Y. Harikane et al. 2023; H. B. Akins et al. 2025; I. Labbe et al. 2025). These LRDs are characterized by broad emission lines (J. Matthee et al. 2024; J. E. Greene et al. 2024; V. Kokorev et al. 2024; D. D. Kocevski et al. 2025; A. J. Taylor et al. 2025), yet they lack detectable X-ray (D. D. Kocevski et al. 2023; M. Yue et al. 2024; I. Juodžbalis et al. 2024; T. T. Ananna et al. 2024; R. Maiolino et al. 2025; H. B. Akins et al. 2025), radio emission (A. J. Gloudemans et al. 2025; K. Perger et al. 2025; G. Mazzolari et al. 2026), and variablities (W. L. Tee et al. 2025; Z. Zhang et al. 2025a; M. Kokubo & Y. Harikane 2025; Z. Stone et al. 2025; C. J. Burke et al. 2025; Z. Liu et al. 2026) with a hand-

Email: tanik@g.fpu.ac.jp

ful of exceptions (L. J. Furtak et al. 2025; X. Ji et al. 2025; Z. Zhang et al. 2025b; R. P. Naidu et al. 2025; F. D'Eugenio et al. 2026). Two primary interpretations for LRDs have emerged: (i) the "BH envelope model," where massive BHs are embedded within dense gas envelopes (A. de Graaff et al. 2025; R. P. Naidu et al. 2025; D. Kido et al. 2025; V. Rusakov et al. 2026), and (ii) the "star-only model," which invokes extremely dense stellar systems (A. Loeb 2024; C. A. Guia et al. 2024; J. F. W. Baggen et al. 2024; H. B. Akins et al. 2025). Even within the framework of the BH envelope model, dense stellar systems may be necessary to explain the ultraviolet continua of LRDs (K. Inayoshi et al. 2026), and may supply gas to a BH envelope through tidal disruption events (K. Kritos & J. Silk 2026). In such extreme environments, a sequence of processes – from runaway stellar collisions to VMS formation and the subsequent creation of massive BHs – is likely inevitable (F. Pacucci et al. 2025; A. Escala et al. 2025).

The collapse of a VMS, particularly one with high spin, may produce detectable electromagnetic (EM) and gravitational-wave (GW) transients. A rapidly spinning VMS is expected to form a BH surrounded by a massive accretion disk immediately following pair instability. Such a BH-disk system may launch relativistic jets (C. L. Fryer et al. 2001; Y. Suwa & K. Ioka 2011; T. Matsumoto et al. 2015) and trigger explosions driven by viscous angular momentum transport (H. Uchida et al. 2019). Furthermore, the massive accretion disk is susceptible to non-axisymmetric instabilities, leading to the emission of burst GWs. Recent studies (M. Shibata et al. 2021; M. Shibata & S. Fujibayashi 2026) suggest that such VMS collapses could explain enigmatic GW transients like GW190521 (R. Abbott et al. 2020a) and GW231123 (A. G. Abac et al. 2025). These events involve BH masses that fall within the so-called pair-instability mass gap (R. Abbott et al. 2020b; R. Farmer et al. 2020; S. E. Woosley & A. Heger 2021; A. K. Mehta et al. 2022; E. Farag et al. 2022), assuming that they originate from genuine BH mergers. Runaway collisions provide a viable mechanism for forming such highly spinning VMSs, as the stellar spin is significantly enhanced by the orbital angular momentum of the colliding progenitors.

In this paper, we investigate runaway collisions and VMS formation within dense star clusters, focusing on two primary objectives. First, we track the evolution of the spin angular momentum of VMSs formed in these clusters. This analysis is crucial to determine whether VMS collapse can trigger the EM and GW transients proposed in recent literature. Second, we incorporate the effects of stellar bloating on VMS growth. Collision products are expected to remain bloated over the Kelvin-Helmholtz (KH) timescale. If a VMS experiences successive collisions within this timeframe, it maintains an expanded radius and a low effective temperature of ~ 5000 K at the so-called Hayashi track (T. Hosokawa et al. 2012, 2013). Such a bloated VMS possesses a significantly larger cross-section, facilitating further collisions. To our knowledge, this bloating effect has not been fully accounted for in previous numerical simulations of runaway collisions. Although M. Fujii et al. (2009) considered the core-halo structure of VMSs, their models assumed temperatures exceeding 2×10^4 K (M. Ishii et al. 1999), which remain considerably higher than the values expected for a fully bloated state at the Hayashi track.

The remainder of this paper is organized as follows. In Section 2, we describe our numerical methodology and physical assumptions. In Section 3, we present the results of our N-body simulations. Section 4 provides a discussion on the implications for the EM and GW counterparts produced by the collapse of highly spinning VMSs. Finally, we summarize our conclusions in Section 5. Throughout this paper, c and G denote the speed of light and gravitational constant, respectively.

2. METHOD

We perform N-body simulations to investigate four types of dense star clusters with distinct initial conditions. The common characteristics of these models are as follows. For the initial phase-space density, we adopt the King model with a concentration parameter of $W_0 = 12$ (I. R. King 1966). We do not account for initial mass segregation or fractal configurations. Clusters are assumed to be isolated, meaning that they are not embedded within the tidal field of a host galaxy. The initial binary fraction is set to 0%. We adopt a cluster metallicity of $Z = 2 \times 10^{-3}$ ($0.1\,Z_\odot$), since LRDs may be metal-poor (L. R. Ivey et al. 2026). These four cluster types vary in their initial stellar mass functions (IMFs), total masses, and initial mass densities within their half-mass radii, as summarized in Table 1. Regarding stellar populations, we employ two types of IMFs. The first is the Kroupa IMF (P. Kroupa 2001), with minimum and maximum stellar masses of $0.08\,M_\odot$ and $150\,M_\odot$, respectively. The second is a "top-heavy" IMF defined as

$$\frac{dN}{dm} \propto m^{-1} \quad (10 \leq m/M_\odot \leq 150), \tag{1}$$

where N and m denote the stellar number and mass, respectively, which is inspired by IMFs in low-metalicity and high-redshift environments (S. Chon et al. 2021, 2022).

The initial mass density within the half-mass radius of our cluster models ranges from 10^6 to $10^7\,M_\odot\,\mathrm{pc}^{-3}$ (see the column $\rho_{\rm h,i}$ in Table 1), which are higher than those typically observed in the Milky Way and other nearby galaxies. According to S. F. Portegies Zwart et al. (2010) and M. R. Krumholz et al. (2019), the mass densities of such observed clusters rarely exceed $10^6\,M_\odot\,\mathrm{pc}^{-3}$, even in the most extreme cases. Our cluster models are intended to represent the central regions of the progenitor clusters of LRDs. Consequently, as detailed below, while their mass densities are comparable to or even higher than those of LRDs, their total masses remain smaller than the LRD scale.

Within the framework of the star-only model, mass densities of 10^4–$10^5\,M_\odot\,\mathrm{pc}^{-3}$ within 1 pc are typical values for LRDs, as derived by J. F. W. Baggen et al. (2024) and C. A. Guia et al. (2024). It is important to note that the number of massive stars in the top-heavy IMF exceeds that of the Kroupa IMF by a factor of 2 for stars with $> 10\,M_\odot$ and by a factor of 15 for stars with $> 100\,M_\odot$. The mass-to-light ratio of a cluster with a top-heavy IMF is a factor of 10 smaller than that of a cluster with a Kroupa IMF; for a given total mass, the former is 10 times brighter than the latter. Although the actual mass density within 1 pc of the top-heavy cluster is $\sim 10^4$–$10^5\,M_\odot\,\mathrm{pc}^{-3}$, it should be regarded as equivalent to $\sim 10^5$–$10^6\,M_\odot\,\mathrm{pc}^{-3}$ when comparing it with the aforementioned literature. Notably, a significant fraction of LRDs ($\sim 20\%$) exhibit such high mass densities (C. A. Guia et al. 2024). In the context of a BH envelope model, star clusters associated with LRDs are estimated to have $\sim 10^8$–$10^{10}\,M_\odot$ within $\lesssim 100$ pc (D. D. Kocevski et al. 2025), corresponding to $\sim$ 20–2000 $M_\odot\,\mathrm{pc}^{-3}$. While our cluster models appear to have much higher mass densities than those typically associated with LRDs in this model, it should be noted that the observed sizes of LRD-associated clusters are upper limits; consequently, their derived mass densities represent lower limits. Furthermore, since our cluster models are significantly less massive than these observed systems, our simulations effectively represent the dense central regions of such clusters as progenitors of LRDs. This reasoning also applies to the star-only model, where the total star cluster masses reach $\sim 10^8$–$10^9\,M_\odot$.

We follow the dynamics of these clusters using the N-body simulation code `PETAR` (L. Wang et al. 2020a). `PETAR` is highly optimized for parallel computing via `FDPS` (M. Iwasawa et al. 2016, 2020) and accurately resolves few-body orbits using the `SDAR` algorithm (L. Wang et al. 2020b). The code handles single and binary stellar evolution through the `BSE` package (J. R. Hurley et al. 2000, 2002; S. Banerjee et al. 2020), which

Table 1. Initial conditions and VMS results of 4 clusters.

Model	$N_{\rm i}$	$M_{\rm i}$	$\rho_{\rm h,i}$	$\rho_{\rm 1pc,i}$	$t_{\rm rh,i}$	$t_{\rm dyn}$	IMF	VMS bloated	VMS mass	VMS radius	VMS spin
		[$M_\odot$]	[$M_\odot\,\mathrm{pc}^{-3}$]	[$M_\odot\,\mathrm{pc}^{-3}$]	[year]	[year]			[$M_\odot$]	[GM/c^2]	[GM^2/c]
M5D6K-N	1.7×10^5	10^5	10^6	2.4×10^4	1.1×10^7	4.3×10^4	Kroupa	No	1200	1.7×10^4	28
M5D7K-N	1.7×10^5	10^5	10^7	2.4×10^4	3.4×10^6	1.3×10^4	Kroupa	No	2200	1.6×10^4	10
M5D7H-N	2.0×10^3	10^5	10^7	2.4×10^4	6.7×10^4	2.2×10^4	Top-heavy	No	4400	1.4×10^4	10
M6D7H-N	1.9×10^4	10^6	10^7	2.4×10^5	4.8×10^5	1.6×10^5	Top-heavy	No	24000	4.8×10^3	4.0
M5D6K-Y	1.7×10^5	10^5	10^6	2.4×10^4	1.1×10^7	4.3×10^4	Kroupa	Yes	5000	2.0×10^6	56
M5D7K-Y	1.7×10^5	10^5	10^7	2.4×10^4	3.4×10^6	1.3×10^4	Kroupa	Yes	8600	1.7×10^6	14
M5D7H-Y	2.0×10^3	10^5	10^7	2.4×10^4	6.7×10^4	2.2×10^4	Top-heavy	Yes	19000	1.5×10^6	18
M6D7H-Y	1.9×10^4	10^6	10^7	2.4×10^5	4.8×10^5	1.6×10^5	Top-heavy	Yes	95000	1.2×10^6	6.5

NOTE—$N_{\rm i}$, $M_{\rm i}$, $\rho_{\rm h,i}$, $\rho_{\rm 1pc,i}$, and $t_{\rm rh,i}$ denotes the number of stars, cluster mass, mass density within half-mass radius, mass density within 1 pc, and half-mass relaxation time at the initial time.

incorporates stellar wind mass loss based on the prescription of K. Belczynski et al. (2010). In our simulations, two stellar wind regimes are particularly prominent: the winds of hot, massive H-rich stars (J. S. Vink et al. 2001) and those of luminous blue variables (LBVs; R. M. Humphreys & K. Davidson 1994). Unlike the analytical approach taken by F. Pacucci et al. (2025), we do not implement specialized mass-loss treatments for VMSs. Furthermore, we assume perfectly sticky collisions, neglecting any loss of mass or angular momentum specifically driven by the stellar collision process itself.

We employ a single-star evolution model that differs from the default prescription in the `BSE` code, which we refer to as the "L model." This model was constructed based on 1D stellar evolution simulations of stars with masses ranging from $8\,M_\odot$ to $1280\,M_\odot$, performed using the `HOSHI` code (K. Takahashi et al. 2016, 2018, 2019; T. Yoshida et al. 2019). The detailed parameter settings and physical assumptions of the L model are described in A. Tanikawa et al. (2020) and A. Tanikawa et al. (2022).

We follow the cluster evolution for 1 Myr after formation, ensuring that all stars remain in the main-sequence (MS) phase throughout the simulations. In our model, a collision between two MS stars is triggered when their separation becomes smaller than the sum of their radii. Upon merging, the collision product undergoes rejuvenation due to the supply of fresh hydrogen to its core. We quantify this rejuvenation process as

$$T_{\rm age,3} = C T_{\rm ms,3} \frac{m_1 (T_{\rm age,1}/T_{\rm ms,1}) + m_2 (T_{\rm age,2}/T_{\rm ms,2})}{m_3} \quad (2)$$

where m_i represents the mass of the i-th star, $T_{\rm ms,i}$ is its MS lifetime, and $T_{\rm age,i}$ is its current age. Here, the indices 1 and 2 denote the progenitor stars ($m_1 \geq m_2$), while the index 3 denotes the resulting collision product (i.e., $m_3 = m_1 + m_2$). The rejuvenation coefficient C is defined as

$$C = \begin{cases} 0.1\,(m_2/m_1 > 0.1) \\ 1.0\,(m_2/m_1 \leq 0.1) \end{cases} . \quad (3)$$

Under this prescription, the collision product is significantly rejuvenated if the progenitor stars have comparable masses, whereas rejuvenation is suppressed for highly unequal-mass collisions. For instance, this prevents unrealistic rejuvenation in collisions between a $1000\,M_\odot$ VMS and a $1\,M_\odot$ star. Note that the original `BSE` code adopts a constant $C = 0.1$ regardless of the mass ratio m_2/m_1, which tends to over-rejuvenate products in encounters with very small ratio, m_2/m_1.

Stellar collisions convert kinetic energy into thermal energy within the resulting collision product. Consequently, the VMS shifts onto the Hayashi track and remains in a bloated state throughout its KH timescale. If a VMS successively accretes other stars within this KH timeframe, it sustains this expanded state (T. Hosokawa et al. 2012, 2013), which in turn increases the cross-section for further stellar collisions.

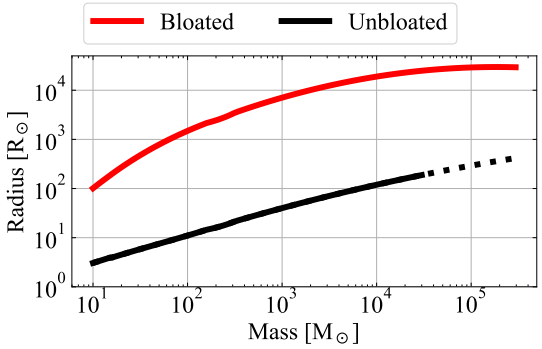

Figure 1. Relation between stellar mass and radius at unbloated and bloated states at the ZAMS time. The dotted curve denotes unbloated radii for > 30000 M$_\odot$. These data points are not utilized, as the VMSs are too compact to be stable to general relativistic instability with mass $\gtrsim 30000$ M$_\odot$ for the unbloated cases.

We model the bloated state of a VMS as follows. Since the maximum initial stellar mass in our clusters is $150\,M_\odot$, any star exceeding $M > 150\,M_\odot$ is considered a collision product. For these objects, we prescribe a persistently bloated state, where the stellar radius is determined by fixing the effective temperature at $T_{\rm eff,bloated} = 5000$ K. In this regime, we assume that the luminosity is preserved from the unbloated state ($L_{\rm bloated} = L_{\rm unbloated}$), where $L_{\rm unbloated}$ is derived from our stellar evolution model without considering the bloated state. Specifically, the bloated radius $R_{\rm bloated}$ is expressed as

$$\left(\frac{R_{\rm bloated}}{R_\odot}\right) = 4.2 \times 10^3 \left(\frac{L_{\rm bloated}}{10^{7.5}\,L_\odot}\right)^{1/2} \left(\frac{T_{\rm eff,bloated}}{T_{\rm eff,\odot}}\right)^{-2} \quad (4)$$

where $T_{\rm eff,\odot} = 5777$ K. As a VMS evolves into a post-MS star, it may expand beyond this radius. Therefore, the actual VMS radius $R_{\rm VMS}$ is given by

$$R_{\rm VMS} = \max(R_{\rm bloated}, R_{\rm unbloated}), \quad (5)$$

where $R_{\rm unbloated}$ represents the radius in the unbloated case[4]. We maintain this bloated state even if the VMS does not undergo a collision strictly within one KH timescale; however, we subsequently perform a post-processing analysis to assess the self-consistency of this assumption.

[4] This is because the effective temperature of a star can fall below 5000 K in our single-star evolution model. However, it does not drop below 5000 K in the current simulations, and $R_{\rm bloated} > R_{\rm unbloated}$ always holds true.

In our post-processing analysis, we evaluate the self-consistency of the bloated state model using three distinct criteria. The first criterion is whether the VMS sustains an accretion rate exceeding $\dot{M}_{\rm crit} = 3 \times 10^{-2}\,M_\odot\,{\rm yr}^{-1}$ (T. Hosokawa et al. 2012, 2013). The remaining two criteria pertain to the KH timescale of the VMS, for which we consider two different physical cases. Specifically, we calculate the KH timescale by adopting either the bloated radius ($R_{\rm bloated}$) or the unbloated radius ($R_{\rm unbloated}$), while maintaining the unbloated luminosity ($L_{\rm unbloated}$) consistently in both cases. These KH timescales are given by

$$\left(\frac{t_{\rm KH,unbloated}}{\rm yr}\right) = 2.5\times10^4 \left(\frac{M}{10^3\,M_\odot}\right)^2 \times \left(\frac{R_{\rm unbloated}}{10^{1.6}\,R_\odot}\right)^{-1} \left(\frac{L_{\rm unbloated}}{10^{7.5}\,L_\odot}\right)^{-1} \quad (6)$$

$$\left(\frac{t_{\rm KH,bloated}}{\rm yr}\right) = 2.0\times10^2 \left(\frac{M}{10^3\,M_\odot}\right)^2 \times \left(\frac{R_{\rm bloated}}{10^{3.7}\,R_\odot}\right)^{-1} \left(\frac{L_{\rm unbloated}}{10^{7.5}\,L_\odot}\right)^{-1} \quad (7)$$

The use of $t_{\rm KH,unbloated}$ as a criterion may be physically justified because the bulk of the VMS mass remains centrally concentrated, even when the envelope is bloated (T. Hosokawa et al. 2012, 2013).

The collision criterion for a bloated VMS is identical to that used for standard MS-MS collisions: a collision is triggered when the separation between two stars becomes smaller than the sum of their radii. We assume that these collisions are perfectly sticky, resulting in no mass loss, and that the orbital angular momentum of the progenitor binary is entirely partitioned into the spin angular momentum of the collision product. It should be noted, however, that since a VMS likely possesses a distinct core-envelope structure, a stellar collision could potentially strip the envelope. In such a scenario, the orbital angular momentum might not be fully converted into the spin of the resulting VMS. By adopting the current assumption of full conversion and zero mass loss, our model effectively provides an upper limit for both the mass and spin growth of the VMS.

Figure 1 illustrates the relationship between stellar mass and radius for zero-age main-sequence (ZAMS) stars in both unbloated and bloated states. As shown, the bloated radii approach a constant value for masses $\gtrsim 10^5\,{\rm M}_\odot$. This unreasonable thing happens for the following reason. Our single-star evolution model is based on fitting formulae derived from 1D simulation results for stars ranging from $8\,{\rm M}_\odot$ to $1280\,{\rm M}_\odot$. While these formulae are extrapolated to the extremely high-mass regime, it should be noted that this extrapolation may no longer be physically robust for stars exceeding $\gtrsim 10^5\,{\rm M}_\odot$.

For each initial condition, we conduct two separate simulations: one applying the bloated state to collision products and another omitting it. These cases are labeled as "Yes" or "No" in the "VMS bloated" column of Table 1, and are further distinguished by the suffixes "Y" and "N" in their respective model names. In total, we perform eight simulation runs.

3. RESULTS

Runaway collisions occur in all our models, and VMS masses exceed 1000 ${\rm M}_\odot$, as the dynamical friction timescale for the most massive stars is sufficiently shorter than their or VMS evolutionary timescales[5]. The dynamical friction timescale can be expressed as

$$t_{\rm dyn} \sim \frac{m_{\rm ave,i}}{m_{\rm heavy,i}} t_{\rm rh,i}, \quad (8)$$

where $m_{\rm heavy,i}$ and $m_{\rm ave,i}$ are the heaviest stellar mass and average mass at the initial time, respectively, and $t_{\rm rh,i}$ is the initial half-mass relaxation time. This initial relaxation time is defined as

$$t_{\rm rh,i} = 0.0477 \frac{N_{\rm i}}{(G\rho_{\rm h,i})^{1/2}\ln(0.4N_{\rm i})}, \quad (9)$$

where $N_{\rm i}$ and $\rho_{\rm h,i}$ denote the initial number of stars and the initial half-mass density, respectively. The dynamical friction timescale for models M6D7H can be written as

$$t_{\rm dyn} \sim 1.6\times10^5 \left(\frac{m_{\rm ave}}{0.59\ {\rm M}_\odot}\right) \times \left(\frac{m_{\rm heavy}}{150\ {\rm M}_\odot}\right)^{-1} \left(\frac{t_{\rm rh,i}}{11\ {\rm Myr}}\right)\ [{\rm yr}]. \quad (10)$$

Note that models M6D7H have the longest dynamical friction timescale among our models (see Table 1). The dynamical friction timescale is much shorter than the VMS evolution timescale ($\sim$ 3 Myr). In general, the core relaxation time is used as the criterion for the onset of runaway collisions. In this study, however, we adopt the half-mass relaxation time because the stars contributing to the runaway process originated largely from outside the initial core. This is evident from the

[5] If this hierarchy of timescales is reversed, runaway collisions become unlikely. In such cases, massive stars evolve into BHs before they can sink to the cluster center. Once formed, BHs have a collisional cross-section that is orders of magnitude smaller than that of stars, making further collisions with other stars highly improbable. On the other hand, it has also been pointed out that IMBHs could potentially form through pathways distinct from runaway collisions (e.g. M. Giersz et al. 2015).

fact that the total mass of stars initially residing within the core accounted for only $\sim 0.5\%$ of the cluster mass, whereas the final VMS mass reaches $\sim$ 1–10% of the total mass.

Figure 2 illustrates the mass evolution of the most massive star (i.e., VMS) within each star cluster. In model M5D7K-N, the VMS mass reaches $2.2 \times 10^3\,\mathrm{M}_\odot$, accounting for approximately 2.2% of the total cluster mass. The VMS grows rapidly during the initial 0.1 Myr, after which the growth rate declines as the cluster expands and becomes more diffuse due to two-body relaxation. By 1 Myr, the mass growth has effectively ceased. In contrast, for model M5D7K-Y, which incorporates the bloated state of the VMS, the growth is significantly enhanced. Due to its increased cross-section, the bloated VMS undergoes mergers more frequently, reaching $\sim 8.6 \times 10^3\,\mathrm{M}_\odot$ (or 8.6% of the cluster mass) by 1 Myr. Beyond this point, the VMS is expected to grow further. The physical validity of adopting this bloated state model is discussed in detail later.

When considering either the bloated or unbloated VMS cases individually, Table 1 reveals that the mass ratio of the VMS to the total cluster mass is consistently anti-correlated with the initial half-mass relaxation time ($t_{\rm rh,i}$). In both scenarios, the mass ratio increases as the initial mass density increases (cf. models M5D6K and M5D7K), as the IMF becomes more top-heavy (cf. models M5D7K and M5D7H), or as the total number of stars decreases (cf. models M5D7H and M6D7H). This consistent trend arises because the runaway collision process is fundamentally driven by two-body relaxation.

The spin angular momenta of the VMSs, normalized to the dimensionless spin parameter, far exceed unity (see Table 1 and Figure 2). These VMS spins can be estimated as follows. The spin angular momentum of a VMS evolves through a random walk, where each step corresponds to the orbital angular momentum contributed by a collided star. The total angular momentum J can be approximated as

$$J \sim N_{\rm coll}^{1/2} \overline{m}_* b \overline{v}, \tag{11}$$

where $N_{\rm coll}$ is the number of stellar collisions, $\overline{m}_*$ is the average mass of a star colliding with the VMS, b is the typical impact parameter, and $\overline{v}$ is the 3D velocity dispersion of the cluster. The impact parameter b can be estimated from the Keplerian limit as

$$b \sim \frac{\sqrt{2 G m_{\rm VMS} R_{\rm VMS}}}{\overline{v}}, \tag{12}$$

where $m_{\rm VMS}$ and $R_{\rm VMS}$ are the mass and radius of the VMS, respectively. Substituting Eq. (12) into Eq. (11), we obtain

$$J \sim N_{\rm coll}^{1/2} \overline{m}_* \sqrt{2 G m_{\rm VMS} R_{\rm VMS}}. \tag{13}$$

Assuming $m_{\rm VMS} \sim N_{\rm coll} \overline{m}_*$, we can rewrite this expression as

$$J \sim m_{\rm VMS} \sqrt{2 G \overline{m}_* R_{\rm VMS}}. \tag{14}$$

Normalizing this result to the dimensionless spin parameter, we find

$$\frac{J}{G m_{\rm VMS}^2 / c} \sim 17 \left(\frac{\overline{m}_*}{10\,\mathrm{M}_\odot} \right)^{1/2} \left(\frac{m_{\rm VMS}}{10^3\,\mathrm{M}_\odot} \right)^{-1} \left(\frac{R_{\rm VMS}}{30\,\mathrm{R}_\odot} \right)^{1/2} \tag{15}$$

where we have adopted the parameters characteristic of model M5D7K-N. In Figure 3, we compare the VMS spins obtained from our simulations with the values estimated using Eq. (15). We find that they are consistent within a factor of a few.

In the following, we examine the simulation results for the cases incorporating the bloated state, with a primary focus on model M6D7H-Y. In this model, the accretion rate of the VMS exceeds $\dot{M}_{\rm crit} = 3 \times 10^{-2}\,\mathrm{M}_\odot\,\mathrm{yr}^{-1}$ during the initial 0.5 Myr. Meanwhile, the time intervals between successive stellar collisions remain shorter than $t_{\rm KH,bloated}$ throughout the first 1 Myr. Our analysis indicates that the criterion that the VMS accretion rate exceeds $M_{\rm crit}$ is the most stringent. If we strictly apply this condition, the bloated state would be maintained only during the initial 0.5 Myr. However, even if the VMS follows our simulation results for the first 0.5 Myr and subsequently ceases its rapid growth by transitioning to an unbloated state, it would still reach a mass of at least $8.4 \times 10^4\,\mathrm{M}_\odot$. This corresponds to approximately 10% of the total cluster mass, which is more than three times larger than the mass attained in a scenario where the VMS remains unbloated throughout its entire evolution.

For the three remaining models other than M6D7H-Y, the time intervals between successive collisions are shorter than $t_{\rm KH,unbloated}$ but longer than $t_{\rm KH,bloated}$ (see Figure 2). Furthermore, the accretion rate of the VMS exceeds $\dot{M}_{\rm crit} = 3 \times 10^{-2}\,\mathrm{M}_\odot\,\mathrm{yr}^{-1}$ only during the initial ~ 0.01 Myr, suggesting that the bloated phase may not be long-lasting in these cases. Nevertheless, the VMS mass at 0.01 Myr in the bloated case is already larger than the mass at 1 Myr in the unbloated case by 50% (model M5D7K-Y) and 100% (model M5D7H-Y). These results suggest that accounting for the bloated state is essential for understanding VMS growth within the typical mass densities of LRDs.

Finally, we compare our results with several previous simulations of extremely dense star clusters resembling LRDs. F. Pacucci et al. (2025) reported the

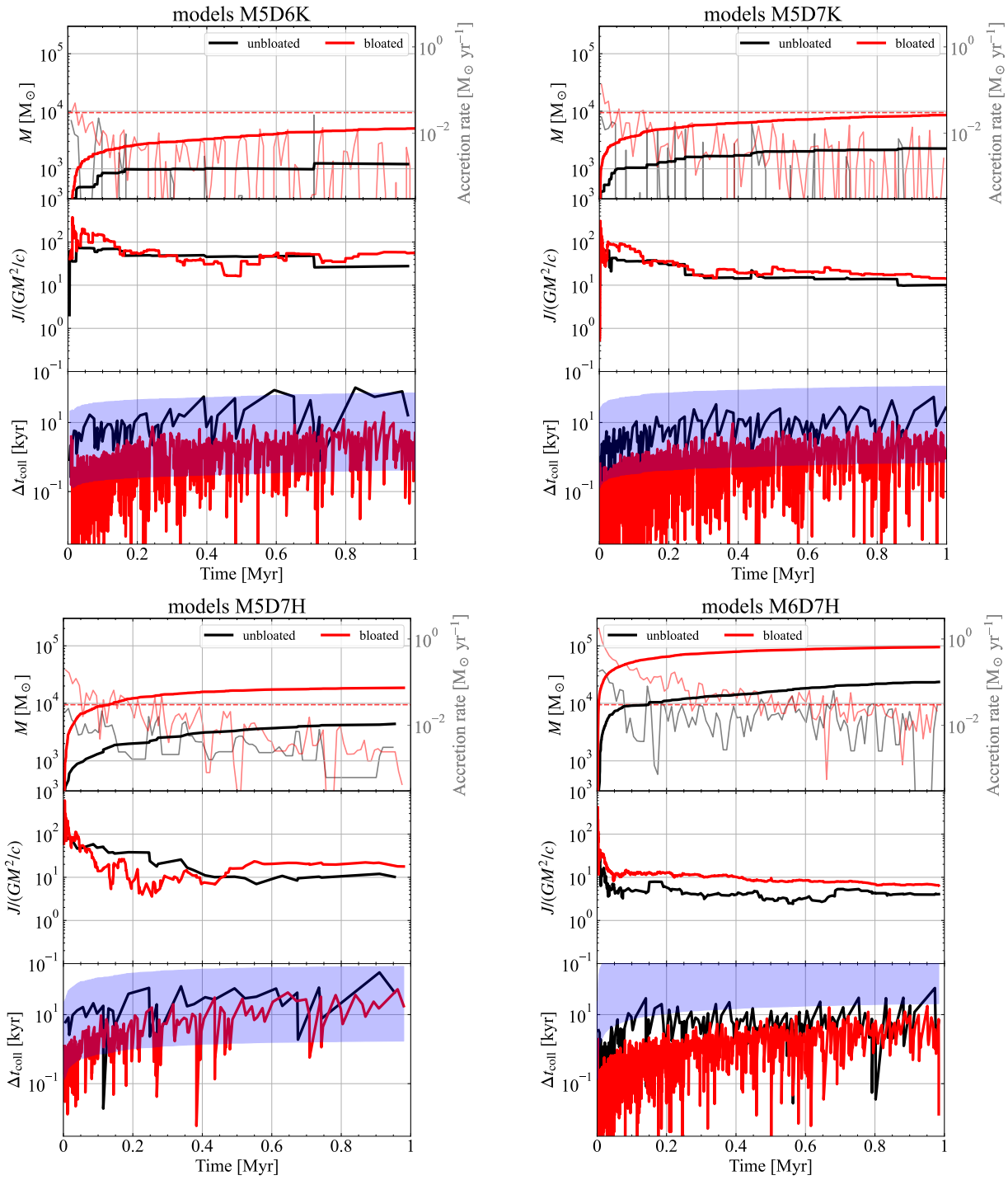

Figure 2. Time evolution of VMS masses, accretion rates, dimensionless spins, and time intervals between collisions for each model. Black and red curves indicate unbloated and bloated models, respectively. Thin grey and red curves in the top panels indicate VMS mass accretion rates in the unbloated and bloated cases, respectively. The shaded regions in the bottom panels show regions sandwiched between the minimum and maximum of KH timescales, i.e. $t_{\rm KH,bloated}$ and $t_{\rm KH,unbloated}$, respectively (see Eq. (7) and Eq. (6)). The dashed lines indicate an accretion rate of $\dot{M}_{\rm crit} = 3 \times 10^{-2}$ M$_\odot$ yr^{-1}, which is the lower limit for keeping the bloated states suggested by T. Hosokawa et al. (2012, 2013).

formation of $\sim 10^4$ M$_\odot$ VMSs within star clusters of $\sim 6 \times 10^5$ M$_\odot$. They found that the accretion rate remains below $\dot{M}_{\rm crit} = 3 \times 10^{-2}$ M$_\odot$ yr^{-1} over 1 Myr, leading to their conclusion that accounting for the bloated state of the VMS is unnecessary. The discrepancy between their findings and our results primarily arises from

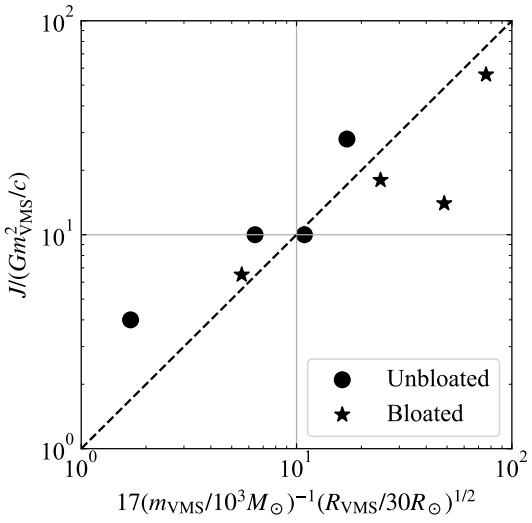

Figure 3. Relation between VMS spins in simulation results, and estimated with Eq. (15). These values are equal on the dashed line. Circles and star marks indicate the unbloated and bloated cases, respectively. We assume $m_* = 10\ \mathrm{M}_\odot$.

the difference in the initial mass density of the star clusters. While F. Pacucci et al. (2025) consider a central mass density of $\sim 10^7\,\mathrm{M}_\odot\,\mathrm{pc}^{-3}$, our simulations employ a density of $\sim 10^7\,\mathrm{M}_\odot\,\mathrm{pc}^{-3}$ within the half-mass radius; consequently, the central mass density in our models is significantly higher than $10^7\,\mathrm{M}_\odot\,\mathrm{pc}^{-3}$. Furthermore, M. C. Vergara et al. (2025) identified a VMS exceeding $5\times10^4\,\mathrm{M}_\odot$ in a $\sim 6\times10^5\,\mathrm{M}_\odot$ star cluster with a half-mass radius density of $\sim 7\times10^7\,\mathrm{M}_\odot\,\mathrm{pc}^{-3}$, which is much higher than our cluster models. Although they did not incorporate the bloated state, it is possible that the VMS in their model would satisfy the criteria for such a state.

4. DISCUSSIONS

It should be noted that the VMS masses and spins obtained in our simulations represent upper limits, as several mass and angular momentum loss processes were not explicitly modeled. Stellar collisions themselves can induce mass loss; therefore, the mass of a collision product may be less than the combined mass of the two pre-collision stars (M. Freitag & W. Benz 2005). Assuming that a VMS rotates rigidly, we compare the VMS rotation frequency (ω) with the Kepler rotation frequency ($\omega_{\rm k}$):

$$\frac{\omega}{\omega_{\rm k}} = \frac{J/(km_{\rm VMS}R_{\rm VMS}^2)}{\sqrt{Gm_{\rm VMS}/R_{\rm VMS}^3}} \sim \sqrt{2}k^{-1}\overline{m}_*^{1/2}m_{\rm VMS}^{-1/2}$$
$$\sim 1.09\left(\frac{k}{0.075}\right)^{-1}\left(\frac{\overline{m}_*}{10\ \mathrm{M}_\odot}\right)^{1/2}\left(\frac{m_{\rm VMS}}{3\times10^3\ \mathrm{M}_\odot}\right)^{-1/2} \quad (16)$$

Here, k denotes the moment of inertia coefficient. The second equality is derived by substituting Eq. (13) into the expression for J. For the third equality, we adopt $k = 0.075$, which corresponds to a polytrope with index $n = 3$ or, equivalently, a radiative sphere. Since the VMS rotation frequency exceeds a few 10 % of the Kepler rotation frequency, mass shedding is likely to happen during the evolution of VMSs from hydrogen burning to helium and carbon burning phases in which the stellar core becomes compact (see below).

A similar reduction likely applies to the spin angular momentum of the VMSs. Furthermore, we do not account for stellar winds specifically associated with VMSs (J. S. Vink 2018), nor do we consider the potentially enhanced stellar winds unique to the bloated state (D. Nakauchi et al. 2020). During the post-MS phases, these VMSs are expected to lose significant mass and angular momentum via stellar winds, particularly if successive collisions partially eject their hydrogen envelopes.

The dimensionless spin parameter of each VMS is found to be of order 10. VMSs evolve from the MS phase to helium and carbon burning ones, eventually forming an oxygen-carbon core surrounded by an extended hydrogen and helium envelope (K. Takahashi et al. 2018). The oxygen-carbon core finally becomes unstable to the electron-positron pair creation instability if the core mass is smaller than $10^4 M_\odot$ (M. Shibata et al. 2025), and if the core mass is large enough ($\gtrsim 140 M_\odot$), a BH would be formed. The dimensionless spin for the oxygen-carbon core is unlikely to be as large as ~ 10 because of the angular momentum transport during the stellar evolution (K. Takahashi et al. 2018), but even when it is 1–2, the remnant after the collapse is likely to be a rapidly spinning BH surrounded by a massive accretion disk (M. Shibata & S. Fujibayashi 2026). Such BH-accretion disk systems are capable of driving explosions fueled by viscous heating and angular momentum transport (H. Uchida et al. 2019), and may launch jets exhibiting ultra-long gamma-ray bursts (Y. Suwa & K. Ioka 2011; T. Matsumoto et al. 2015) if the jets can penetrate the massive envelope. These could be EM transients. Furthermore, these massive accretion disks may experience one-armed spiral instabilities, emitting burst GWs similar to those associated with GW190521 and GW231123 (M. Shibata et al. 2021; M. Shibata & S. Fujibayashi 2026). Consequently, the collapse of a highly spinning VMS could manifest as a multi-messenger transient.

Note that the VMS reaches a mass of at least $8.4\times10^4\,\mathrm{M}_\odot$ in the MS stage for model M6D7H-Y. Such a star should be categorized as a supermassive star (SMS), which is subject to general-relativistic radial instability

(I. Iben 1963; S. Chandrasekhar 1964; Y. B. Zeldovich & I. D. Novikov 1971; S. L. Shapiro & S. A. Teukolsky 1983; G. M. Fuller et al. 1986). The collapse of an SMS may also be observed as an EM transient (C. Jockel et al. 2025). Regardless of its spin parameter, an SMS is believed to undergo a thermonuclear explosion if the metallicity is high with $Z \gtrsim 0.005$ (K. J. Fricke 1973; G. M. Fuller et al. 1986; P. J. Montero et al. 2012; C. Nagele et al. 2020, 2022, 2023; C. Nagele & H. Umeda 2024) or if the SMS mass has a particular mass (K.-J. Chen et al. 2014). If an SMS is rapidly rotating, a strong shock wave is expected to form within the accreting material surrounding the BH remnant, driving a powerful outflow (W. H. Lee & E. Ramirez-Ruiz 2006; Y. T. Liu et al. 2007; H. Uchida et al. 2017; S. Fujibayashi et al. 2025).

We note that it remains non-trivial whether these VMSs/SMSs rotate rigidly. Since their spin angular momentum is primarily contributed by stellar collisions, it is possible that only their stellar envelopes are rapidly rotating, and thus, mass loss due to the stellar wind may be more serious. To rigorously assess whether these VMSs/SMSs undergo rigid rotation, three-dimensional hydrodynamics simulations would be required to investigate the effect of angular momentum transport. Recent numerical simulations have suggested that collisions between MS stars amplify the magnetic fields of the resulting products (F. R. N. Schneider et al. 2019; T. Ryu et al. 2025; S. T. Ohlmann et al. 2025). Such magnetic fields may facilitate the transport of angular momentum from the stellar envelope to the core. In any case, our cluster simulation results highlight the possibility that VMSs/SMSs formed in dense star clusters could be eventually observed as EM and GW transients, powered by the resulting BH-accretion disk systems. Even if they do not explode, they could potentially become a quasi-star or a BH envelope and grow into LRDs. At this time, the envelope rotates sub-Keplerianly.

5. CONCLUSIONS

We have investigated the mass and spin growth of VMSs in dense star clusters using gravitational N-body simulations, with parameters inspired by clusters potentially associated with LRDs. Our models incorporate the bloated state of a VMS at the Hayashi track resulting from successive stellar collisions. We find that a single VMS typically grows to $\sim 10^3$–$10^4\,\mathrm{M}_\odot$ in each cluster. Depending on the cluster parameters, the inclusion of the bloated state enhances VMS growth by several tens of percent to several times. This demonstrates the necessity of accounting for the bloated phase when investigating VMS evolution in environments resembling LRDs. Furthermore, these VMSs are rapidly rotating, with dimensionless spin parameters of ~ 10 across all investigated models. This high spin is well-explained by the conversion of the orbital angular momentum of collided stars into the spin angular momentum of the VMS.

The masses and spins of these VMSs satisfy the necessary conditions for rotation-driven EM and GW transients, which could be observable after the collapse of the VMSs. A highly spinning VMS is expected to undergo an explosion driven by a BH-accretion disk system formed upon its collapse. Such systems are also potential sources of burst GWs, similar to those associated with GW190521 and GW231123. Or possibly, they could become a quasi-star or a BH envelope and grow into LRDs.

Several physical processes were not explicitly included in this study, such as mass and angular momentum loss during stellar collisions, the internal redistribution of spin angular momentum, and post-MS evolution. Incorporating these effects will be the next crucial step in refining our understanding of VMS mass and spin evolution.

ACKNOWLEDGMENTS

This research is supported partly by Grants-in-Aid for Scientific Research, 22H00130 (KI), 23H04900 (MS and KI), 23H05430(KI), 23H01172 (KI), 24K07040 (AT), 25K01035 (AT), and 26H02045 (KI). AT also thanks for the Step-up program at Fukui Prefectural University. Numerical simulations are carried out on the Yukawa Institute Computer Facility. We started this study thanks to the YITP workshop "Exploring Extreme Transients 2025" (YITP-W-25-08).

AUTHOR CONTRIBUTIONS

A. Tanikawa performed the calculations, analyzed the data, produced the figures, and led the manuscript writing. All authors contributed to scientific discussion and manuscript writing.

REFERENCES

Abac, A. G., Abouelfettouh, I., Acernese, F., et al. 2025, ApJL, 993, L25, doi: 10.3847/2041-8213/ae0c9c

Abbott, R., Abbott, T. D., Abraham, S., et al. 2020a, PhRvL, 125, 101102, doi: 10.1103/PhysRevLett.125.101102

Abbott, R., Abbott, T. D., Abraham, S., et al. 2020b, ApJL, 900, L13, doi: 10.3847/2041-8213/aba493
Akins, H. B., Casey, C. M., Lambrides, E., et al. 2025, ApJ, 991, 37, doi: 10.3847/1538-4357/ade984
Ananna, T. T., Bogdán, Á., Kovács, O. E., Natarajan, P., & Hickox, R. C. 2024, ApJL, 969, L18, doi: 10.3847/2041-8213/ad5669
Baggen, J. F. W., van Dokkum, P., Brammer, G., et al. 2024, ApJL, 977, L13, doi: 10.3847/2041-8213/ad90b8
Banerjee, S., Belczynski, K., Fryer, C. L., et al. 2020, A&A, 639, A41, doi: 10.1051/0004-6361/201935332
Begelman, M. C., & Rees, M. J. 1978, MNRAS, 185, 847, doi: 10.1093/mnras/185.4.847
Belczynski, K., Bulik, T., Fryer, C. L., et al. 2010, ApJ, 714, 1217, doi: 10.1088/0004-637X/714/2/1217
Burke, C. J., Stone, Z., Shen, Y., & Jiang, Y.-F. 2025, arXiv e-prints, arXiv:2511.16082, doi: 10.48550/arXiv.2511.16082
Chandrasekhar, S. 1964, ApJ, 140, 417, doi: 10.1086/147938
Chen, K.-J., Heger, A., Woosley, S., et al. 2014, ApJ, 790, 162, doi: 10.1088/0004-637X/790/2/162
Chon, S., Omukai, K., & Schneider, R. 2021, MNRAS, 508, 4175, doi: 10.1093/mnras/stab2497
Chon, S., Ono, H., Omukai, K., & Schneider, R. 2022, MNRAS, 514, 4639, doi: 10.1093/mnras/stac1549
de Graaff, A., Rix, H.-W., Naidu, R. P., et al. 2025, A&A, 701, A168, doi: 10.1051/0004-6361/202554681
D'Eugenio, F., Juodžbalis, I., Ji, X., et al. 2026, MNRAS, 545, staf2117, doi: 10.1093/mnras/staf2117
Di Carlo, U. N., Mapelli, M., Pasquato, M., et al. 2021, MNRAS, 507, 5132, doi: 10.1093/mnras/stab2390
Escala, A., Zimmermann, L., Valdebenito, S., et al. 2025, ApJ, 995, 44, doi: 10.3847/1538-4357/ae200e
Farag, E., Renzo, M., Farmer, R., Chidester, M. T., & Timmes, F. X. 2022, ApJ, 937, 112, doi: 10.3847/1538-4357/ac8b83
Farmer, R., Renzo, M., de Mink, S. E., Fishbach, M., & Justham, S. 2020, ApJL, 902, L36, doi: 10.3847/2041-8213/abbadd
Farrell, S. A., Webb, N. A., Barret, D., Godet, O., & Rodrigues, J. M. 2009, Nature, 460, 73, doi: 10.1038/nature08083
Freitag, M., & Benz, W. 2005, MNRAS, 358, 1133, doi: 10.1111/j.1365-2966.2005.08770.x
Fricke, K. J. 1973, ApJ, 183, 941, doi: 10.1086/152280
Fryer, C. L., Woosley, S. E., & Heger, A. 2001, ApJ, 550, 372, doi: 10.1086/319719
Fujibayashi, S., Jockel, C., Kawaguchi, K., Sekiguchi, Y., & Shibata, M. 2025, ApJ, 981, 119, doi: 10.3847/1538-4357/adb0b8
Fujii, M., Iwasawa, M., Funato, Y., & Makino, J. 2009, ApJ, 695, 1421, doi: 10.1088/0004-637X/695/2/1421
Fujii, M. S., Wang, L., Tanikawa, A., Hirai, Y., & Saitoh, T. R. 2024, Science, 384, 1488, doi: 10.1126/science.adi4211
Fuller, G. M., Woosley, S. E., & Weaver, T. A. 1986, ApJ, 307, 675, doi: 10.1086/164452
Furtak, L. J., Secunda, A. R., Greene, J. E., et al. 2025, A&A, 698, A227, doi: 10.1051/0004-6361/202554110
Giersz, M., Leigh, N., Hypki, A., Lützgendorf, N., & Askar, A. 2015, MNRAS, 454, 3150, doi: 10.1093/mnras/stv2162
Gloudemans, A. J., Duncan, K. J., Eilers, A.-C., et al. 2025, ApJ, 986, 130, doi: 10.3847/1538-4357/adddb9
González Prieto, E., Kremer, K., Fragione, G., et al. 2022, ApJ, 940, 131, doi: 10.3847/1538-4357/ac9b0f
Greene, J. E., Labbe, I., Goulding, A. D., et al. 2024, ApJ, 964, 39, doi: 10.3847/1538-4357/ad1e5f
Guia, C. A., Pacucci, F., & Kocevski, D. D. 2024, Research Notes of the American Astronomical Society, 8, 207, doi: 10.3847/2515-5172/ad7262
Häberle, M., Neumayer, N., Seth, A., et al. 2024, Nature, 631, 285, doi: 10.1038/s41586-024-07511-z
Harikane, Y., Zhang, Y., Nakajima, K., et al. 2023, ApJ, 959, 39, doi: 10.3847/1538-4357/ad029e
Heger, A., & Woosley, S. E. 2002, ApJ, 567, 532, doi: 10.1086/338487
Hosokawa, T., Omukai, K., & Yorke, H. W. 2012, ApJ, 756, 93, doi: 10.1088/0004-637X/756/1/93
Hosokawa, T., Yorke, H. W., Inayoshi, K., Omukai, K., & Yoshida, N. 2013, ApJ, 778, 178, doi: 10.1088/0004-637X/778/2/178
Humphreys, R. M., & Davidson, K. 1994, PASP, 106, 1025, doi: 10.1086/133478
Hurley, J. R., Pols, O. R., & Tout, C. A. 2000, MNRAS, 315, 543, doi: 10.1046/j.1365-8711.2000.03426.x
Hurley, J. R., Tout, C. A., & Pols, O. R. 2002, MNRAS, 329, 897, doi: 10.1046/j.1365-8711.2002.05038.x
Iben, Jr., I. 1963, ApJ, 138, 1090, doi: 10.1086/147708
Inayoshi, K., Murase, K., & Kashiyama, K. 2026, ApJ, 1000, 90, doi: 10.3847/1538-4357/ae42ce
Ishii, M., Ueno, M., & Kato, M. 1999, PASJ, 51, 417, doi: 10.1093/pasj/51.4.417
Ivey, L. R., D'Eugenio, F., Maiolino, R., et al. 2026, arXiv e-prints, arXiv:2604.09177, doi: 10.48550/arXiv.2604.09177
Iwasawa, M., Namekata, D., Nitadori, K., et al. 2020, PASJ, 72, 13, doi: 10.1093/pasj/psz133
Iwasawa, M., Tanikawa, A., Hosono, N., et al. 2016, PASJ, 68, 54, doi: 10.1093/pasj/psw053

Ji, X., Maiolino, R., Übler, H., et al. 2025, MNRAS, 544, 3900, doi: 10.1093/mnras/staf1867
Jockel, C., Kawaguchi, K., Fujibayashi, S., & Shibata, M. 2025, Mon. Not. Roy. Astron. Soc., 545, staf1949, doi: 10.1093/mnras/staf1949
Juodžbalis, I., Ji, X., Maiolino, R., et al. 2024, MNRAS, 535, 853, doi: 10.1093/mnras/stae2367
Kido, D., Ioka, K., Hotokezaka, K., Inayoshi, K., & Irwin, C. M. 2025, MNRAS, 544, 3407, doi: 10.1093/mnras/staf1898
King, I. R. 1966, AJ, 71, 64, doi: 10.1086/109857
Kocevski, D. D., Onoue, M., Inayoshi, K., et al. 2023, ApJL, 954, L4, doi: 10.3847/2041-8213/ace5a0
Kocevski, D. D., Finkelstein, S. L., Barro, G., et al. 2025, ApJ, 986, 126, doi: 10.3847/1538-4357/adbc7d
Kokorev, V., Caputi, K. I., Greene, J. E., et al. 2024, ApJ, 968, 38, doi: 10.3847/1538-4357/ad4265
Kokubo, M., & Harikane, Y. 2025, ApJ, 995, 24, doi: 10.3847/1538-4357/ae119e
Kritos, K., & Silk, J. 2026, ApJL, 1000, L21, doi: 10.3847/2041-8213/ae4c52
Kroupa, P. 2001, MNRAS, 322, 231, doi: 10.1046/j.1365-8711.2001.04022.x
Krumholz, M. R., McKee, C. F., & Bland -Hawthorn, J. 2019, ARA&A, 57, 227, doi: 10.1146/annurev-astro-091918-104430
Labbe, I., Greene, J. E., Bezanson, R., et al. 2025, ApJ, 978, 92, doi: 10.3847/1538-4357/ad3551
Lee, W. H., & Ramirez-Ruiz, E. 2006, ApJ, 641, 961, doi: 10.1086/500533
Liu, Y. T., Shapiro, S. L., & Stephens, B. C. 2007, PhRvD, 76, 084017, doi: 10.1103/PhysRevD.76.084017
Liu, Z., Naidu, R. P., Secunda, A., et al. 2026, arXiv e-prints, arXiv:2604.13000, doi: 10.48550/arXiv.2604.13000
Loeb, A. 2024, Research Notes of the American Astronomical Society, 8, 182, doi: 10.3847/2515-5172/ad614c
Maiolino, R., Risaliti, G., Signorini, M., et al. 2025, MNRAS, 538, 1921, doi: 10.1093/mnras/staf359
Matsumoto, H., Tsuru, T. G., Koyama, K., et al. 2001, ApJ, 547, L25, doi: 10.1086/318878
Matsumoto, T., Nakauchi, D., Ioka, K., Heger, A., & Nakamura, T. 2015, ApJ, 810, 64, doi: 10.1088/0004-637X/810/1/64
Matthee, J., Naidu, R. P., Brammer, G., et al. 2024, ApJ, 963, 129, doi: 10.3847/1538-4357/ad2345
Mazzolari, G., Gilli, R., Maiolino, R., et al. 2026, A&A, 706, A372, doi: 10.1051/0004-6361/202453317
Mehta, A. K., Buonanno, A., Gair, J., et al. 2022, ApJ, 924, 39, doi: 10.3847/1538-4357/ac3130
Montero, P. J., Janka, H.-T., & Müller, E. 2012, ApJ, 749, 37, doi: 10.1088/0004-637X/749/1/37
Nagele, C., & Umeda, H. 2024, PhRvD, 110, L061301, doi: 10.1103/PhysRevD.110.L061301
Nagele, C., Umeda, H., & Takahashi, K. 2023, MNRAS, 523, 1629, doi: 10.1093/mnras/stad1522
Nagele, C., Umeda, H., Takahashi, K., Yoshida, T., & Sumiyoshi, K. 2020, MNRAS, 496, 1224, doi: 10.1093/mnras/staa1636
Nagele, C., Umeda, H., Takahashi, K., Yoshida, T., & Sumiyoshi, K. 2022, MNRAS, 517, 1584, doi: 10.1093/mnras/stac2495
Naidu, R. P., Matthee, J., Katz, H., et al. 2025, arXiv e-prints, arXiv:2503.16596, doi: 10.48550/arXiv.2503.16596
Nakauchi, D., Inayoshi, K., & Omukai, K. 2020, ApJ, 902, 81, doi: 10.3847/1538-4357/abb463
Ohlmann, S. T., Schneider, F. R. N., Roepke, F. K., et al. 2025, arXiv e-prints, arXiv:2512.13424, doi: 10.48550/arXiv.2512.13424
Pacucci, F., Hernquist, L., & Fujii, M. 2025, ApJ, 994, 40, doi: 10.3847/1538-4357/ae1619
Perger, K., Fogasy, J., Frey, S., & Gabányi, K. É. 2025, A&A, 693, L2, doi: 10.1051/0004-6361/202452422
Portegies Zwart, S. F., Baumgardt, H., Hut, P., Makino, J., & McMillan, S. L. W. 2004, Nature, 428, 724, doi: 10.1038/nature02448
Portegies Zwart, S. F., McMillan, S. L. W., & Gieles, M. 2010, ARA&A, 48, 431, doi: 10.1146/annurev-astro-081309-130834
Quinlan, G. D., & Shapiro, S. L. 1990, ApJ, 356, 483, doi: 10.1086/168856
Rizzuto, F. P., Naab, T., Spurzem, R., et al. 2021, MNRAS, 501, 5257, doi: 10.1093/mnras/staa3634
Rusakov, V., Watson, D., Nikopoulos, G. P., et al. 2026, Nature, 649, 574, doi: 10.1038/s41586-025-09900-4
Ryu, T., Sills, A., Pakmor, R., de Mink, S., & Mathieu, R. 2025, ApJL, 980, L38, doi: 10.3847/2041-8213/adaf94
Sanders, R. H. 1970, ApJ, 162, 791, doi: 10.1086/150711
Schneider, F. R. N., Ohlmann, S. T., Podsiadlowski, P., et al. 2019, Nature, 574, 211, doi: 10.1038/s41586-019-1621-5
Shapiro, S. L., & Teukolsky, S. A. 1983, Black holes, white dwarfs, and neutron stars : the physics of compact objects
Shibata, M., & Fujibayashi, S. 2026, ApJ, 996, 57, doi: 10.3847/1538-4357/ae22d4

Shibata, M., Fujibayashi, S., Jockel, C., & Kawaguchi, K. 2025, Astrophys. J., 978, 58, doi: 10.3847/1538-4357/ad93a4

Shibata, M., Kiuchi, K., Fujibayashi, S., & Sekiguchi, Y. 2021, PhRvD, 103, 063037, doi: 10.1103/PhysRevD.103.063037

Stone, Z., Shen, Y., Zhuang, M.-Y., et al. 2025, arXiv e-prints, arXiv:2509.19585, doi: 10.48550/arXiv.2509.19585

Suwa, Y., & Ioka, K. 2011, ApJ, 726, 107, doi: 10.1088/0004-637X/726/2/107

Takahashi, K., Sumiyoshi, K., Yamada, S., Umeda, H., & Yoshida, T. 2019, ApJ, 871, 153, doi: 10.3847/1538-4357/aaf8a8

Takahashi, K., Yoshida, T., & Umeda, H. 2018, ApJ, 857, 111, doi: 10.3847/1538-4357/aab95f

Takahashi, K., Yoshida, T., Umeda, H., Sumiyoshi, K., & Yamada, S. 2016, MNRAS, 456, 1320, doi: 10.1093/mnras/stv2649

Tanikawa, A., Yoshida, T., Kinugawa, T., Takahashi, K., & Umeda, H. 2020, MNRAS, 495, 4170, doi: 10.1093/mnras/staa1417

Tanikawa, A., Yoshida, T., Kinugawa, T., et al. 2022, ApJ, 926, 83, doi: 10.3847/1538-4357/ac4247

Taylor, A. J., Finkelstein, S. L., Kocevski, D. D., et al. 2025, ApJ, 986, 165, doi: 10.3847/1538-4357/add15b

Tee, W. L., Fan, X., Wang, F., & Yang, J. 2025, ApJL, 983, L26, doi: 10.3847/2041-8213/adc5e3

Uchida, H., Shibata, M., Takahashi, K., & Yoshida, T. 2019, ApJ, 870, 98, doi: 10.3847/1538-4357/aaf39e

Uchida, H., Shibata, M., Yoshida, T., Sekiguchi, Y., & Umeda, H. 2017, PhRvD, 96, 083016, doi: 10.1103/PhysRevD.96.083016

Vergara, M. C., Askar, A., Kamlah, A. W. H., et al. 2025, A&A, 704, A321, doi: 10.1051/0004-6361/202555307

Vink, J. S. 2018, A&A, 615, A119, doi: 10.1051/0004-6361/201832773

Vink, J. S., de Koter, A., & Lamers, H. J. G. L. M. 2001, A&A, 369, 574, doi: 10.1051/0004-6361:20010127

Wang, L., Iwasawa, M., Nitadori, K., & Makino, J. 2020a, MNRAS, 497, 536, doi: 10.1093/mnras/staa1915

Wang, L., Nitadori, K., & Makino, J. 2020b, MNRAS, 493, 3398, doi: 10.1093/mnras/staa480

Wang, L., Tanikawa, A., & Fujii, M. 2022, MNRAS, 515, 5106, doi: 10.1093/mnras/stac2043

Woosley, S. E., & Heger, A. 2021, ApJL, 912, L31, doi: 10.3847/2041-8213/abf2c4

Yoshida, T., Takiwaki, T., Kotake, K., et al. 2019, ApJ, 881, 16, doi: 10.3847/1538-4357/ab2b9d

Yue, M., Eilers, A.-C., Ananna, T. T., et al. 2024, ApJL, 974, L26, doi: 10.3847/2041-8213/ad7eba

Zeldovich, Y. B., & Novikov, I. D. 1971, Relativistic astrophysics. Vol.1: Stars and relativity

Zhang, Z., Jiang, L., Liu, W., & Ho, L. C. 2025a, ApJ, 985, 119, doi: 10.3847/1538-4357/adcb3e

Zhang, Z., Li, M., Oguri, M., et al. 2025b, arXiv e-prints, arXiv:2512.05180, doi: 10.48550/arXiv.2512.05180